Defense Threat Reduction Agency
8725 John J. Kingman Road, MS
6201 Fort Belvoir, VA 22060-6201

TECHNICAL REPORT

Structural Origins of Scintillation: Metal Organic Frameworks as a Nanolaboratory

June 2016

F. Patrick Doty et al.

Prepared by:
Sandia National Laboratories
7011 East Avenue
Livermore, CA 94550

REPORT DOCUMENTATION PAGE

Public reporting burden for this collection of information is estimated to average 1 hour per response, including the time for reviewing instructions, searching existing data sources, gathering and maintaining the data needed, and completing and reviewing this collection of information. Send comments regarding this burden estimate or any other aspect of this collection of information, including suggestions for reducing this burden to Department of Defense, Washington Headquarters Services, Directorate for Information Operations and Reports (0704-0188), 1215 Jefferson Davis Highway, Suite 1204, Arlington, VA 22202-4302. Respondents should be aware that notwithstanding any other provision of law, no person shall be subject to any penalty for failing to comply with a collection of information if it does not display a currently valid OMB control number. **PLEASE DO NOT RETURN YOUR FORM TO THE ABOVE ADDRESS.**

1. REPORT DATE *(DD-MM-YYYY)*	2. REPORT TYPE	3. DATES COVERED *(From - To)*

4. TITLE AND SUBTITLE

5a. CONTRACT NUMBER

5b. GRANT NUMBER

5c. PROGRAM ELEMENT NUMBER

6. AUTHOR(S)

5d. PROJECT NUMBER

5e. TASK NUMBER

5f. WORK UNIT NUMBER

7. PERFORMING ORGANIZATION NAME(S) AND ADDRESS(ES)

8. PERFORMING ORGANIZATION REPORT NUMBER

9. SPONSORING / MONITORING AGENCY NAME(S) AND ADDRESS(ES)

10. SPONSOR/MONITOR'S ACRONYM(S)

11. SPONSOR/MONITOR'S REPORT NUMBER(S)

12. DISTRIBUTION / AVAILABILITY STATEMENT

13. SUPPLEMENTARY NOTES

14. ABSTRACT

15. SUBJECT TERMS

16. SECURITY CLASSIFICATION OF:			17. LIMITATION OF ABSTRACT	18. NUMBER OF PAGES	19a. NAME OF RESPONSIBLE PERSON
a. REPORT	b. ABSTRACT	c. THIS PAGE			19b. TELEPHONE NUMBER *(include area code)*

UNIT CONVERSION TABLE
U.S. customary units to and from international units of measurement[*]

U.S. Customary Units	Multiply by → ← Divide by[†]		International Units
Length/Area/Volume			
inch (in)	2.54	$\times 10^{-2}$	meter (m)
foot (ft)	3.048	$\times 10^{-1}$	meter (m)
yard (yd)	9.144	$\times 10^{-1}$	meter (m)
mile (mi, international)	1.609 344	$\times 10^{3}$	meter (m)
mile (nmi, nautical, U.S.)	1.852	$\times 10^{3}$	meter (m)
barn (b)	1	$\times 10^{-28}$	square meter (m^2)
gallon (gal, U.S. liquid)	3.785 412	$\times 10^{-3}$	cubic meter (m^3)
cubic foot (ft^3)	2.831 685	$\times 10^{-2}$	cubic meter (m^3)
Mass/Density			
pound (lb)	4.535 924	$\times 10^{-1}$	kilogram (kg)
unified atomic mass unit (amu)	1.660 539	$\times 10^{-27}$	kilogram (kg)
pound-mass per cubic foot (lb ft^{-3})	1.601 846	$\times 10^{1}$	kilogram per cubic meter (kg m^{-3})
pound-force (lbf avoirdupois)	4.448 222		newton (N)
Energy/Work/Power			
electron volt (eV)	1.602 177	$\times 10^{-19}$	joule (J)
erg	1	$\times 10^{-7}$	joule (J)
kiloton (kt) (TNT equivalent)	4.184	$\times 10^{12}$	joule (J)
British thermal unit (Btu) (thermochemical)	1.054 350	$\times 10^{3}$	joule (J)
foot-pound-force (ft lbf)	1.355 818		joule (J)
calorie (cal) (thermochemical)	4.184		joule (J)
Pressure			
atmosphere (atm)	1.013 250	$\times 10^{5}$	pascal (Pa)
pound force per square inch (psi)	6.984 757	$\times 10^{3}$	pascal (Pa)
Temperature			
degree Fahrenheit (^{o}F)	[T(^{o}F) − 32]/1.8		degree Celsius (^{o}C)
degree Fahrenheit (^{o}F)	[T(^{o}F) + 459.67]/1.8		kelvin (K)
Radiation			
curie (Ci) [activity of radionuclides]	3.7	$\times 10^{10}$	per second (s^{-1}) [becquerel (Bq)]
roentgen (R) [air exposure]	2.579 760	$\times 10^{-4}$	coulomb per kilogram (C kg^{-1})
rad [absorbed dose]	1	$\times 10^{-2}$	joule per kilogram (J kg^{-1}) [gray (Gy)]
rem [equivalent and effective dose]	1	$\times 10^{-2}$	joule per kilogram (J kg^{-1}) [sievert (Sv)]

[*]Specific details regarding the implementation of SI units may be viewed at http://www.bipm.org/en/si/.
[†]Multiply the U.S. customary unit by the factor to get the international unit. Divide the international unit by the factor to get the U.S. customary unit.

2015-11-16

Structural Origins of Scintillation: Metal Organic Frameworks as a Nanolaboratory

The limitations of organic scintillators—nonproportionality to MeV protons, low luminosity and photon transport, and transportation and safety hazards—impose severe practical constraints and raise challenges for fast-neutron detection applications requiring their use. The results of this project provide fundamental insight into the electronic and structural features of novel scintillating materials known as metal organic frameworks (MOFs). The properties of MOF, including nanoporosity, ultrahigh surface areas, ion-induced luminescence, and synthetically flexible structure, present unique advantages for radiation detection over existing organic scintillator materials. In addition, MOFs provide a tailorable "nanolaboratory" for understanding fundamental aspects of the scintillation process in organic-inorganic hybrid scintillators. Key questions that have been addressed include: (1) What processes cause radiation-induced luminescence in MOFs? (2) What factors affect the time-dependent luminescence decay in MOFs, and will, if controlled, lead to MOFs optimized for particle identification and discrimination? (3) Can nanoporous MOFs, by adsorption of fluorophores within their pores, form exciplexes similar to those found in solution-based systems and can these serve as a tool to control the properties of their radiation-induced luminescence?

A combined experimental and theoretical approach was thus employed, utilizing an extensive toolbox of synthetic organic techniques and DFT methods, respectively. Each MOF material was then characterized using a wide variety of optical spectroscopic and X-ray diffraction techniques, including steady-state/time-resolved photoluminescence (PL) and radioluminescence (RL) measurements, electronic absorption spectroscopy, single-crystal X-ray crystallography, and powder XRD. The results provide insight towards the factors that influence the design of these materials for radiation/chemical detection applications, and may be organized into three interrelated categories:

I.   Structural and electronic origins of luminescence/scintillation in MOFs
II. Host-guest interactions and charge-transfer luminescence for radiation/environmental sensing
III. Fast neutron and gamma particle discrimination in MOFs infiltrated with triplet-harvesting complexes

Part I: Structural and electronic origins of luminescence/scintillation in MOFs

Our previous work on two chemically similar but structurally diverse MOFs indicates that the spatial orientation of scintillating groups has a direct effect upon the observed spectral and timing characteristics. A 2-dimensional layered MOF based upon Zn_4O structural nodes and 4,4'-trans-stilbenedicarboxylic acid (H_2SDC) linker groups has been shown to exhibit PL and RL spectra similar to that of the discrete linker group in dilute solution. In contrast, a porous 3-dimensional framework of the same components was shown to possess a dramatically red-shifted RL emission and large Stokes' shift that were not observed in the PL spectra. These observations were attributed to the formation of a dimer-like species that was inaccessible through photoexcitation but accessible upon interaction with ionizing radiation. Furthermore, rigidification of the linker group via chemical bonding to the metal has been shown to decrease the extent of trans-to-cis photoisomerization, which is associated with a higher efficiency of light production and an orders-of-magnitude increase in radiation hardness.

In excess of fifteen additional MOF structures were selected and analyzed to evaluate the generality of these results and to further characterize the structure-property relationships within this new class of scintillators. Initial candidates belonging to the so-called "isoreticular" family of frameworks (IRMOFs) were selected, which refers to a common topological structure for different organic linker groups. Figure 1 illustrates the repeating structural units for a representative set of these complexes, while figure 2 illustrates the different linker groups employed in this study. These systematic changes were performed to not only modify the electronic properties of the scintillating organic groups, but also to change the size of the host cavity. The latter consideration is of particular importance for the development of composite materials via infiltration of guest molecules, as will be discussed in detail in sections (II) and (III).

IRMOF electronic properties were analyzed via DFT to interpret the extent of metal participation in the luminescent states and to elucidate the factors that contribute to favorable scintillation properties such as high luminosity, low self-absorption, and fast timing characteristics. In all cases, closed-shell metal ions such as Zn^{2+}, Cd^{2+}, Al^{3+}, and Zr^{4+} were employed to exclude the possibility of paramagnetic fluorescence quenching. The computational results indicate no participation of the metal orbitals in the framework HOMO and LUMO states, an observation that is supported by experimental results that show linker-centered PL emission for MOFs composed of spatially separated (non-interacting) linker groups. Representative partial density-of-states plots for the terephthalic acid-based IRMOF-1 and the 2-aminoterephthalic acid-based IRMOF-3 are shown in figure 3. In addition to illustrating the non-participation of metal states in the HOMO and LUMO wavefunctions, these figures demonstrate the ability to tune the band-gap though chemical functionalization. In IRMOF-3, the calculated band-gap is 0.7 eV less than that of IRMOF-1 due to the insertion of nitrogen and carbon states within the gap of IRMOF-1. These states are also associated with a shift in the symmetry and extent of electron delocalization in the ground and excited state wavefunctions, which consequently leads to a 60 times higher quantum yield, larger Stokes' shift, and lower emission energy in IRMOF-3.

An additional feature unique to MOFs is the ability to synthesize interpenetrated structural analogs of a variety of basic framework topologies. This provides the ability to systematically modulate the inter-framework spacings and thus the extent of intermolecular interactions between chromophores. One example of such behavior is between the interpenetrated/non-interpenetrated IRMOF-9/IRMOF-10, both of which are composed of tetrahedral Zn_4O nodes and 4,4'-biphenylcarboxylic acid linkers (H_2BPDC). The mode of interpenetration in IRMOF-9 is illustrated schematically in figure 1, for which the nearest-neighbor distance between BPDC linker groups are reduced from 15.44Å to 3.93Å in IRMOFs -10 and -9, respectively. The shorter inter-chromophore distances in IRMOF-9 are associated with the formation of dimer-like species that exhibit wavelength-dependent emission characteristics, longer emission decay time constants, and radioluminescence spectra that are red-shifted relative to the non-interpenetrated IRMOF-10. A similar study was performed for the interpenetrated/non-interpenetrated pair of complexes IRMOF-8(INT)/IRMOF-8, respectively. Both structures comprise 2,6-naphthalenedicarboxylic acid (2,6-NDC) linker groups, and were selected due to the low formation energy and highly emissive properties of naphthalene dimer species. Furthermore, the mode of interpenetration in these complexes (figure 4) differs from that of IRMOFs -9 and -10, allowing for deeper insight into the origin of interchromophore luminescence in MOFs. The nearest-neighbor 2,6-NDC distances range from 4-5 Å, which is consistent with the lowest energy values calculated for this dimer configuration. The observed PL and RL spectra for these structures reveal multiple important properties: (1) scintillation light yields superior to that of the discrete organic linker and other known organic scintillators, (2) superior radiation tolerance relative to crystalline organic scintillators, (3) IRMOF-8 exhibits no excimer emission in PL spectra; equally intense monomer and excimer emission in RL spectra, (4) IRMOF-8(INT) exhibits weak excimer emission in PL spectra; excimer emission is the only observable feature in RL spectra. These combined results indicate that MOFs possess not only notable

advantages over traditional organic scintillators, but also unprecedented structure-dependent interactions with ionizing radiation.

Part II. Host-guest interactions and charge-transfer luminescence for radiation/environmental sensing

The ordered structures and permanent nanoporosity of MOFs render them particularly well suited for the incorporation of guest molecules within the pores. Although this has been performed extensively for the uptake and separation of large number of gases, little is known about the luminescence effects associated with guest uptake. In this work, we have demonstrated the formation of highly luminescent host-guest complexes that are stabilized by the steric and dipolar characteristics of the pore environment. Systematic modification of the host and guest species resulted in composite scintillators tunable with respect to wavelength and timing characteristics. A related finding was the discovery of a new category of solid-state sensor materials that exhibit a ratiometric luminescence response to environmental conditions such as temperature and chemical environment.

An aluminum-based complex based upon 2,6-ndc was selected due to its high stability in a variety of chemical environments and its ability to exhibit dynamic structural distortions in response to guest uptake. This is illustrated in figures 5 and 6, for which transformation from the 'open' (DUT-4) to the 'closed' (MIL-69) form is accomplished according to specific activation procedures that are listed in the appendix. PL and RL spectra collected on these different structures corroborate the results obtained for the interpenetrated/non-interpenetrated IRMOFs, although the extent of interchromophore interaction is much greater in the 'closed' (MIL-69) form. This is due to the nearly idealized dimer geometry of MIL-69, which possesses displaced cofacial orientations of the 2,6-NDC chromophores and a separation of 3.76Å. More surprisingly, powder XRD studies indicate that phases intermediate between the 'open' and 'closed' forms are accessed upon infiltration with different guest molecules. Infiltration with electron-donating species was thus performed to introduce a new electronic charge-transfer (CT) state from which it was possible to perform further tuning of the luminescence properties. The tertiary amines N,N-dimethylamine (DMA) and diethylaniline (DEA) were selected due to their ability to form luminescent exciplexes with electron-accepting organic chromophores. Incorporation of these guests within the pores of DUT-4 was found to result in a slight structural perturbation and stabilization of a ground-state CT complex that does not form in purely organic donor-acceptor systems. The ground-state nature of the CT state was characterized on the basis of the wavelength-dependent emission characteristics and corresponding changes in the excitation spectra, both of which indicate the introduction of a new CT ground state. Long CT emission lifetimes (>30 ns) and unexpectedly large Stokes' shifts (150 nm) were also observed in the MOF-guest complexes, which provides further evidence for the enhanced stability of the guest molecules within the framework pores. Furthermore, the MOF-guest CT state was found to be highly luminescent in all cases, with the emission wavelength determined by the electron affinity of the MOF and ionization potential (IP) of the guest. Excitation emission spectra for DUT-4 (1), MOF-DMA (**1a**) and MOF-DEA (**1b**) are shown in figure 7, for which **1a** exhibits a CT emission maximum of 462nm (DMA IP = 8.14eV), and **1b** at 532nm (DEA IP= 6.99 eV). The corresponding radioluminescence spectra were found to exhibit emission from the monomer, dimer, and CT states (figure 8), which indicates that structural distortion and subsequent dimerization still occur upon ionization of these infiltrated materials.

Temperature-dependent luminescence studies were performed on **1a** and **1b** to further probe the nature of the emissive charge-transfer state. These spectra are summarized in figure 9, which illustrates differing temperature-dependent behavior. Upon controlled heating of complex **1a**, the intensity of the naphthalene monomer emission at 385nm decreased relative to the CT emission at 460nm. In contrast, heating of **1b** led to an increase in the monomer emission to the CT emission at 532nm. The variable-temperature spectra were fit to a sum of weighted Gaussians, and plotted to determine the activation energy of the CT state (figures 10 and 11). The respective reaction enthalpies

for **1a** and **1b** indicate an Arrhenius activated process and a static quenching formation mechanism, respectively. These results also indicate that both of these complexes function as solid-state molecular thermometers that operate ratiometrically. This approach is advantageous over absolute intensity measurements as it does not require extensive calibration and is insensitive to intensity fluctuations at the source. The above observations also confirm the importance of tuning the steric and electronic interactions between the MOF host and guest complex to suit the detection application of interest.

The differing nature of the CT states identified above for **1a** and **1b** also suggests that MOF-guest ground-state complexes could be used in chemical detection schemes based on the chemical nature of the analyte. Although this objective is outside of the scope of the initial project goals, it nevertheless represents an objective relevant to DTRA. We therefore measured the luminescence quenching of these composite materials upon exposure to solvents of different polarities and dielectric constants. The extent of CT luminescence was found to be intimately sensitive to the nature of the solvent, particularly due to the dipolar nature of the CT state and the distance between solvated donor and MOF acceptor species. Although typical solvent polarity chromophores are characterized by solvatochromic shifts in the absorption and emission spectra, these MOF-based materials are characterized by a different behavior. With the exception of chloroform, **1a** and **1b** display a differential quenching response that is dependent upon the nature of the solvent, with response magnitudes that correlate with the Richardt micro-environmental polarity parameter, E_t(30). Clear isosbestic points were observed for all quenchers except chloroform, indicating the specific transition between the locally excited monomer state and ground-state CT emission. An additional unexpected result was the behavior upon exposure to chloroform, in which the luminescence spectra display nonlinear quenching behavior and a 59nm blue-shift in the CT emission maximum (figure 12). These observations are consistent with negative solvato(fluor)chromic behavior, which is quite rate among solvent polarity probes. Furthermore, solvatochromic fluorescence bands are more sensitive to solvent polarity changes than the corresponding absorption bands, although most negative solvatochromic dyes do not exhibit any fluorescence at room temperature. Initial studies using nitrobenzene a surrogate for nitroaromatic explosives detection revealed high detection sensitivity, as evidenced by ratiometric fluorescence quenching at sub- part-per million concentrations. These findings indicate that MOF-guest sensor materials possess great potential for specific sensing applications due to the synthetic flexibility of these donor-acceptor systems and ability to tune the (structural) pore geometry to selectively identify a chemical analyte of interest.

Part III. Fast neutron and gamma particle discrimination in MOFs infiltrated with triplet-harvesting complexes

A fundamental limitation of traditional organic scintillators arises from the limited mobility of triplet states within the scintillator, which adversely reduces the delayed scintillation response and thus the ability to perform neutron/gamma particle discrimination via pulse-shape discrimination (PSD). Unfortunately, the triplet mobility of a material is a highly defect- and structure-sensitive property that is not easily controlled nor understood. Instead, we have defined an alternative approach towards particle discrimination that addresses the limitations of conventional PSD organic scintillators. This approach involves the conversion of intrinsically non-luminescent triplet excited states to highly emissive metal-to-ligand charge transfer triplet states that reside on a heavy-metal guest dopant. In this way, it is possible to exert immense control over the wavelength, timing, and relative luminosity levels of the delayed component of the scintillation pulse. This scheme is summarized in figure 14. Another unprecedented feature of this approach is the ability to spectrally separate the prompt (host) response from the delayed (guest metal complex) response, which enables optical resolution of the particle type according to a method we term Spectral-Shape Discrimination (SSD).

MOFs are uniquely suited as hosts to triplet-harvesting guest complexes, due to their intrinsic scintillation properties, tunable pore sizes, and well-defined crystalline structures. This allows for modification of the MOF cavity to securely capture the heavy-metal dopant such that the interaction distance is minimized and the host-guest triplet energy transfer efficiency is maximized. We have successfully applied these considerations to demonstrate particle discrimination in three different MOFs infiltrated with three different organometallic iridium guest complexes.

The MOFs IRMOF-10, DUT-6, and MOF-177 were selected for infiltration due to their large pore sizes and high scintillation light yields. The pore sizes range from 1.8 nm in IRMOF-10 to 2.8 nm in MOF-177, which coincides with the diameters of the iridium guest complexes shown in figure 16. Infiltration of these frameworks was performed according to 'ship-in-bottle' and solvent-assisted methods. 'Ship-in-bottle' refers to the growth of the MOF lattice around a guest molecule that is too large to fit through the pore windows but small enough to fit within the pore itself. Solvent-assisted infiltration was performed though simple dissolution of the guest molecule in an appropriate solvent and subsequent mixing with the activated MOF. Homogeneous infiltration in both cases was confirmed through ICP-OES and cross-sectional fluorescence microscopy.

A key feature of these infiltrated materials is the ability to independently modify the photophysical properties of both the host framework and guest complex. This is demonstrated in figure 17, which illustrate framework (singlet-based) emission at 385nm and guest (triplet-based emission) at 599nm. Facile modification of the triplet-based emission in a wavelength range of 465-647nm was possible through infiltration with chemically modified guest complexes. An added benefit of this approach involves the luminescence timing characteristics, which are inextricably linked to the nature of the emissive state. The singlet-based host luminescence is a simple fluorescence process with a decay time on the order of several nanoseconds, whereas the triplet-based guest emission is from a metal-to-ligand charge transfer (MLCT) excited state with a decay time on the order of a microsecond or less (figure 18). Figure 19 shows the steady-state radioluminescence spectra obtained for 2.5 MeV protons and 30 keV electrons, which simulate the recoil protons and Compton scattered electrons generated upon exposure to fast neutrons and gamma rays, respectively. The results indicate a particle-dependent spectral response, for which the prompt host fluorescence is quenched relative to the delayed guest-based emission for protons (neutrons) relative to electrons (gammas). This result is analogous to timing-based pulse-shape discrimination (PSD), for which the prompt component of the scintillation response is quenched for high specific energy loss (dE/dX) particles such as protons. However, SSD is distinct in that it allows for particle discrimination solely on the basis of wavelength. A simplified scheme for this method is provided in figure 20, which compares the pulse height response for two photomultiplier tubes separated by dichroic filters that separate the prompt and delayed spectral features. A SSD figure-of-merit (SSD-FOM) was devised as the separation between neutron and gamma events divided by the sum of the full-width at half maximum of the two distributions. This metric is analogous to the PSD-FOM quoted for liquid scintillators, although this value is dependent on the wavelength of the dichroic filters used as opposed to the prompt/delayed timing cut imposed on the scintillation pulse data in PSD. A representative plot of the simulated SSD-FOM is shown in figure 21. These data were obtained by simulating given numbers of detected photons according to a cumulative probability distribution that was defined according to the proton and electron radioluminescence spectra. The obtained values compare favorably to existing commercial liquid scintillators, which possess PSD-FOM values between 2-4 at 1 MeV electron equivalent energy (roughly equivalent to 1000 photons detected in figure 22). Timing-based particle discrimination was also investigated in the above infiltrated MOF materials, as summarized for the scintillation timing distributions shown in figure 23. These data indicate that these materials are also capable of PSD due to the observed differential timing response for different particle types.

The above studies indicate that it is indeed possible to utilize MOFs as a platform from which to exert control over the factors that determine the luminescence response in this new class of organic-based scintillators. We have found that the luminescence properties are independent of the identity of the closed-shell metal ions, although the presence of chemical bonds between the linker and metal ions has been shown to favorably increase both the radiation tolerance and luminescence quantum yields of these materials over their purely organic counterparts. Control over all aspects of the luminescence properties have been demonstrated, ranging from an increase in the quantum yield through chemical substitution to excited-state dimer formation via structural interpenetration. Results obtained from the above fundamental studies were also applied to develop infiltrated materials for environmental sensing and ionizing radiation particle discrimination applications, respectively.

Publications:
Feng, P.L.; Perry, J.J.; Nikodemski, S.; Jacobs, B.W.; Meek, S.T.; Allendorf, M.D. "Assessing the purity of metal-organic frameworks using photoluminescence: MOF-5, ZnO Quantum Dots, and Framework Decomposition" *J. Am. Chem. Soc.* **2010**, 132, 15487.

Feng, P.L.; Branson, J.V.; Hattar, K.; Vizkelethy, G.; Allendorf, M.D.; Doty, F.P. "Designing metal-organic frameworks for radiation detection" *Nucl. Instr. Meth. A* **2011**, 652, 295.

Feng, P.L.; Leong, K.; Allendorf, M.D. "Charge-transfer guest interactions in luminescent MOFs: implications for solid-state temperature and environmental sensing" *Dalton Trans.* **2012**, 41, 8869.

Related and Follow-on Funding:
- Two-color infiltrated MOFs for neutron discrimination (LDRD, $250k/year, FY10)
- MOF-based scintillators (NA-22, ~600k / year, FY10-FY12)
- Triplet-Harvesting doped plastic scintillators (NA-22, 650k/year, FY11-FY13)
- MOF-based photovoltaics (LDRD, ~500k / year, FY12-FY14)
- Sunshot MOF-PV (DOE, ~500 k/ year, FY12-FY14)

Students:
Stefan Nikodemski , Undergraduate at Colorado School of Mines– Summer 2010.
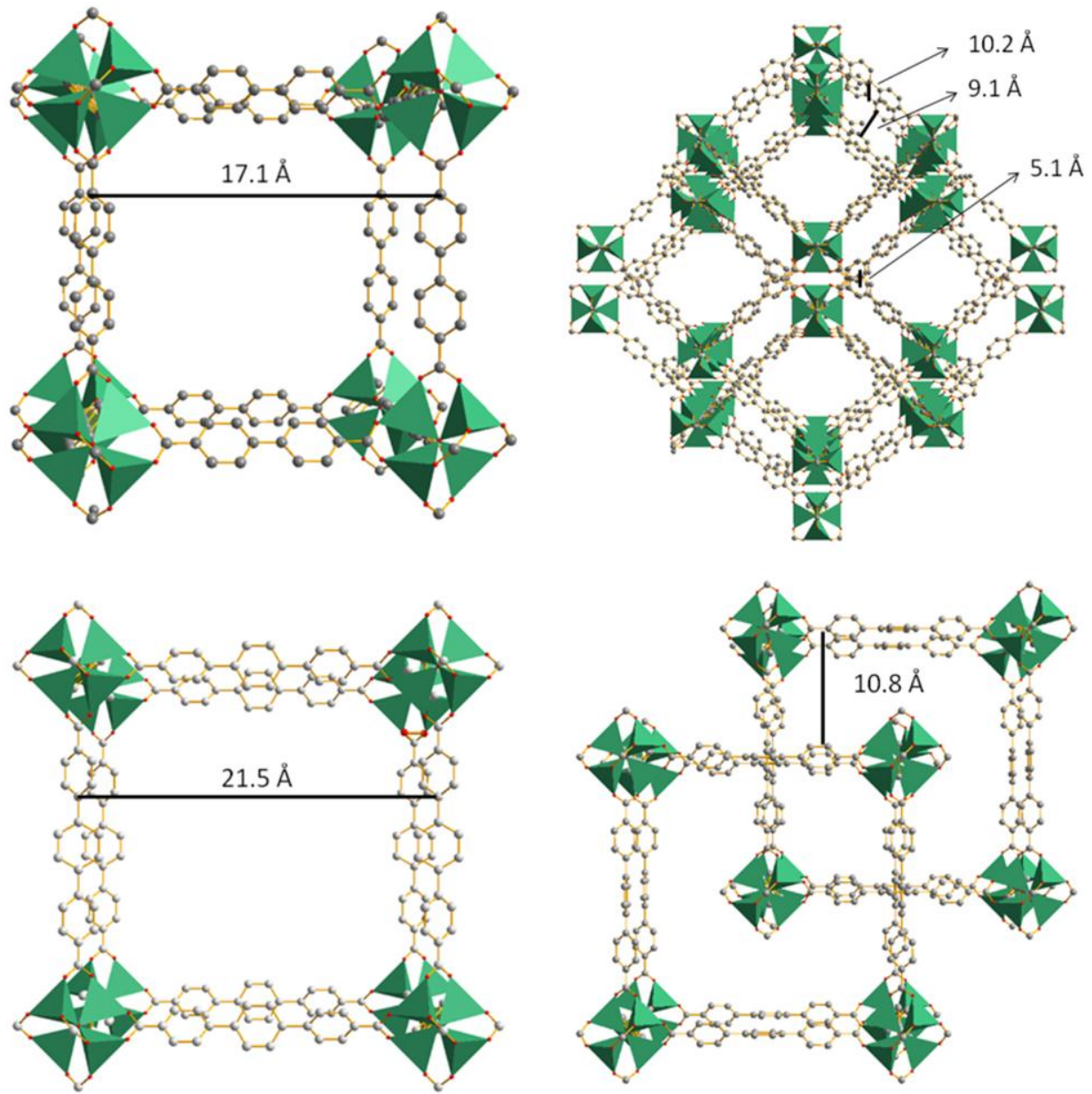
Figure 1. Representative isoreticular MOF structures, illustrating differences in inter-linker spacings and framework catenation (Clockwise starting from top left: IRMOF-9, IRMOF-10, IRMOF-15, IRMOF-16).
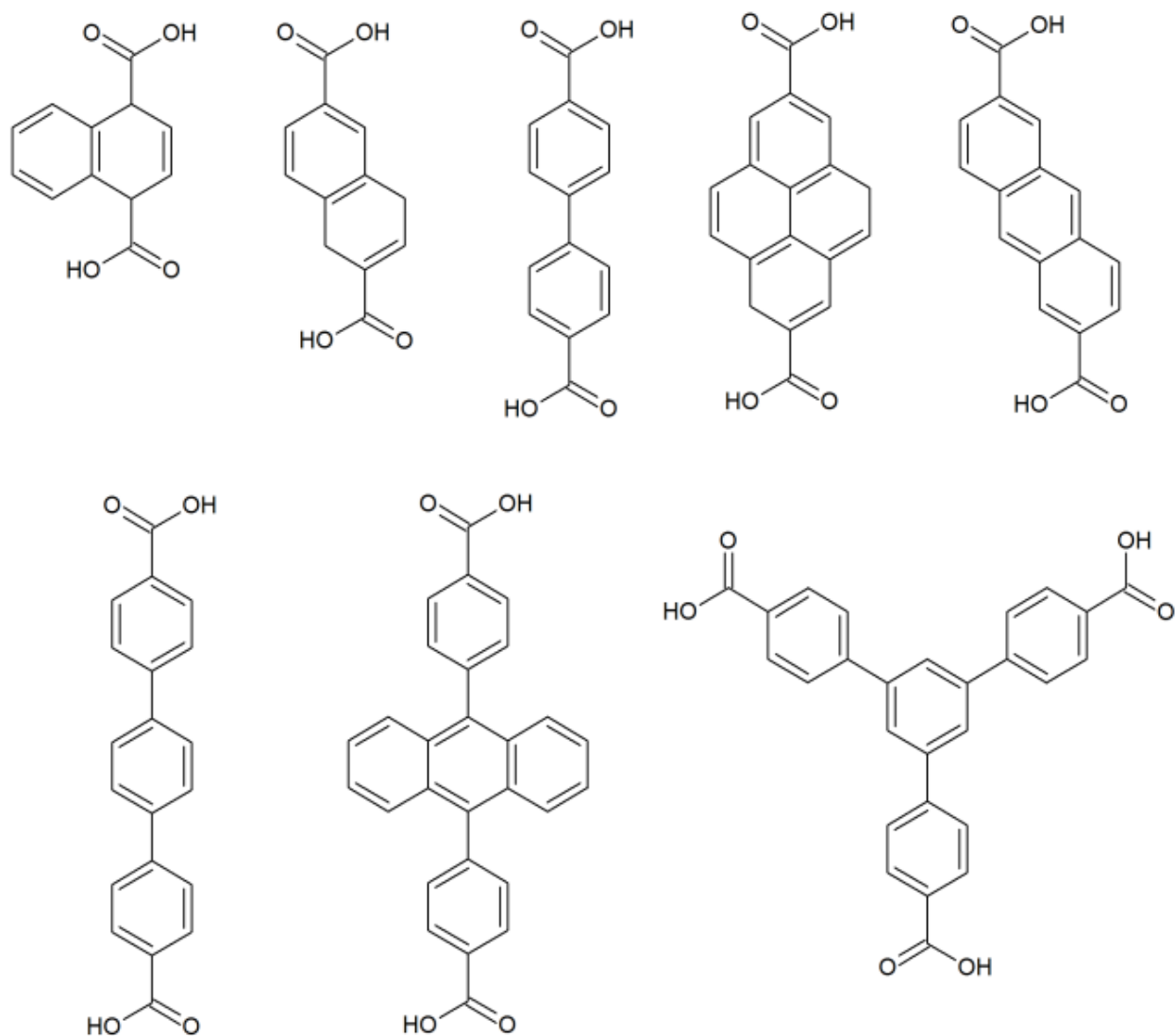
Figure 2. Carboxylic acid linker groups employed in this study.
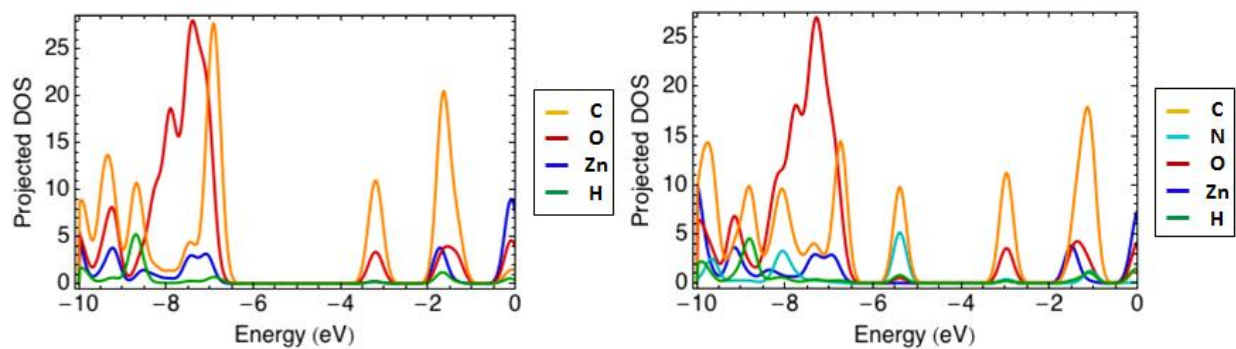
Figure 3. Projected density of states for IRMOF-1 (left) and IRMOF-3 (right).
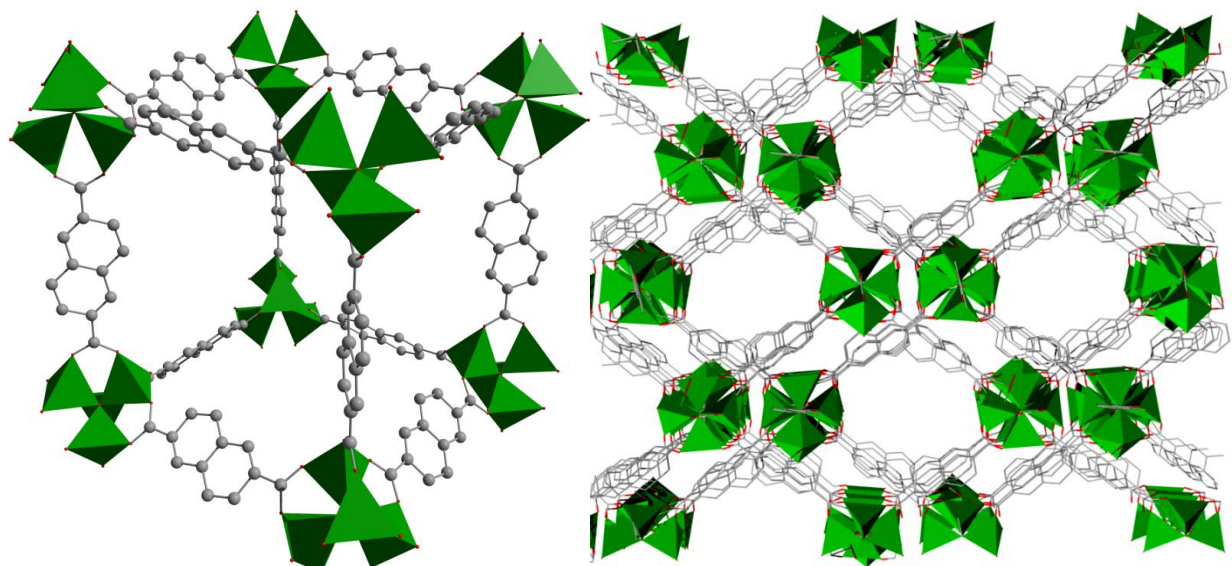
Figure 4. Structures of IRMOF-8 (left) and IRMOF-8(INT) (right).
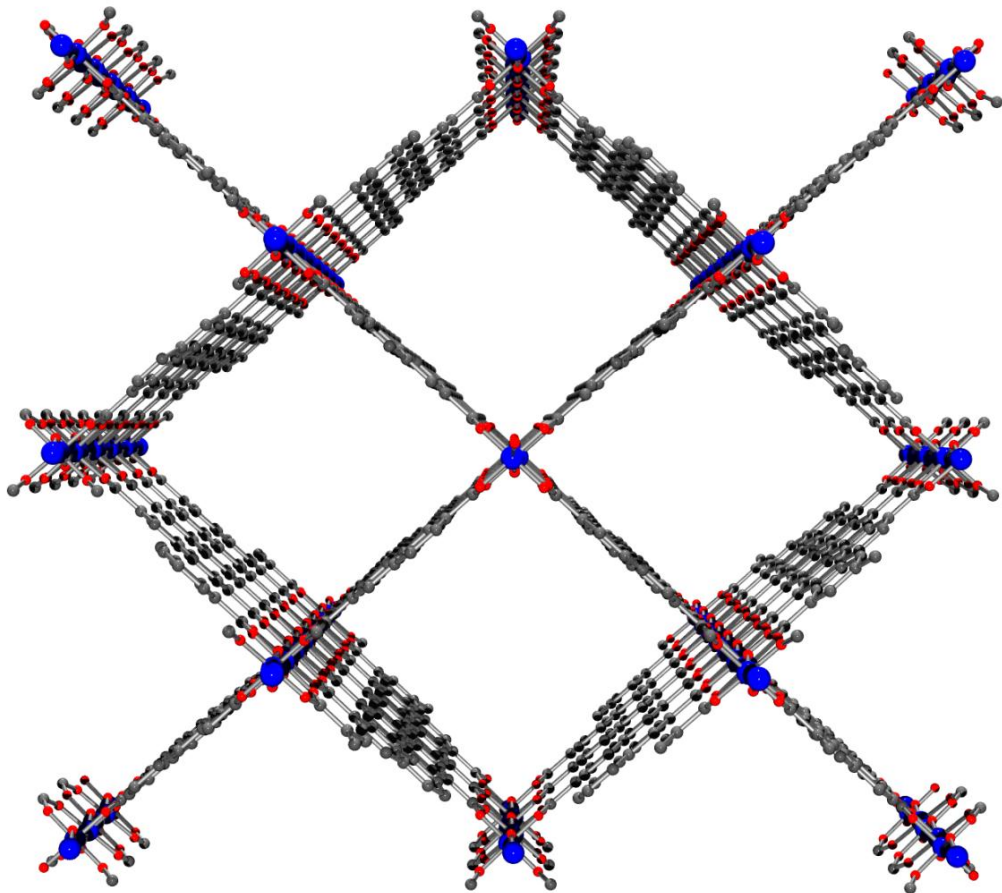
Figure 5. Structure of the 'open' framework DUT-4.
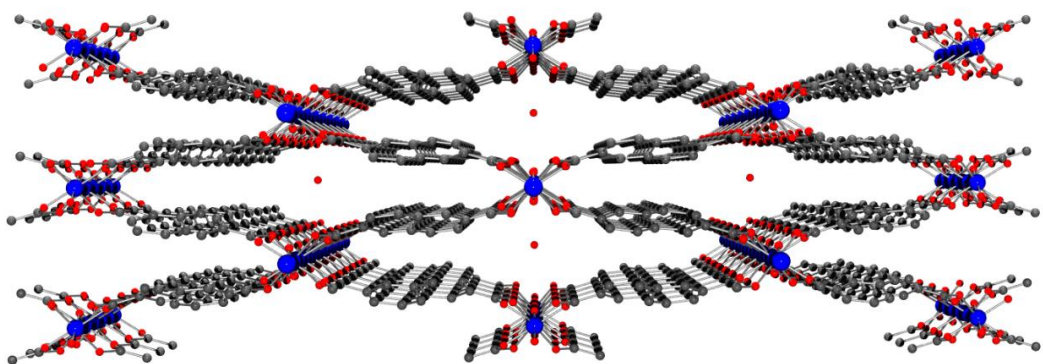
Figure 6. Structure of the 'closed' framework MIL-69.
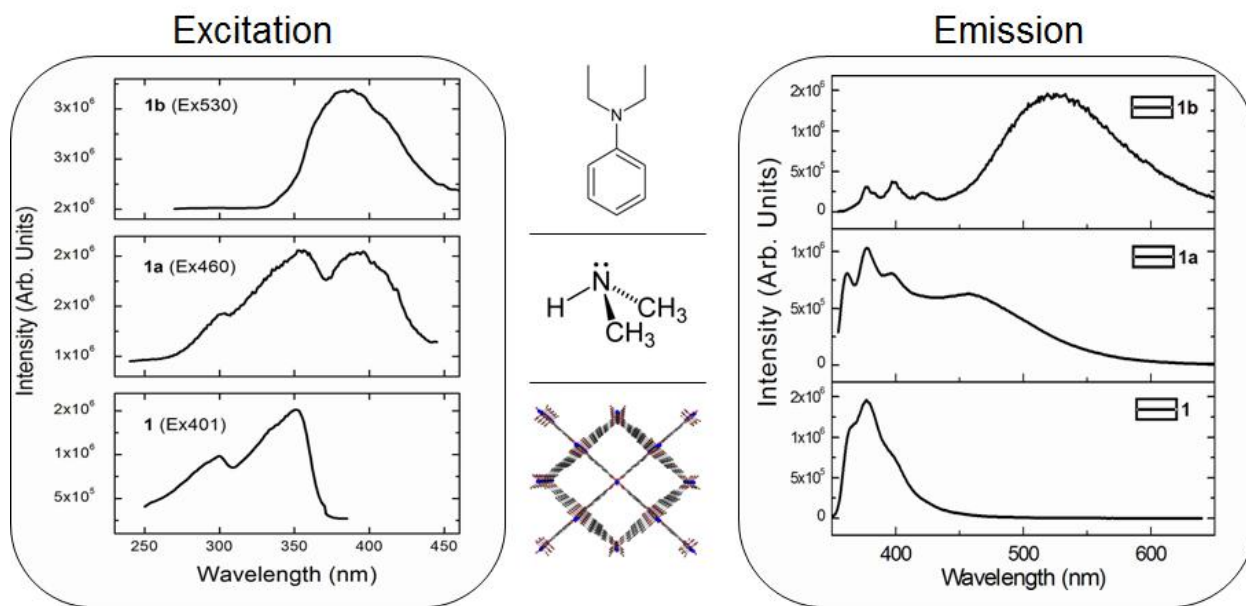
Figure 7. Photoluminescence excitation and emission spectra for complexes **1**, **1a**, and **1b**.
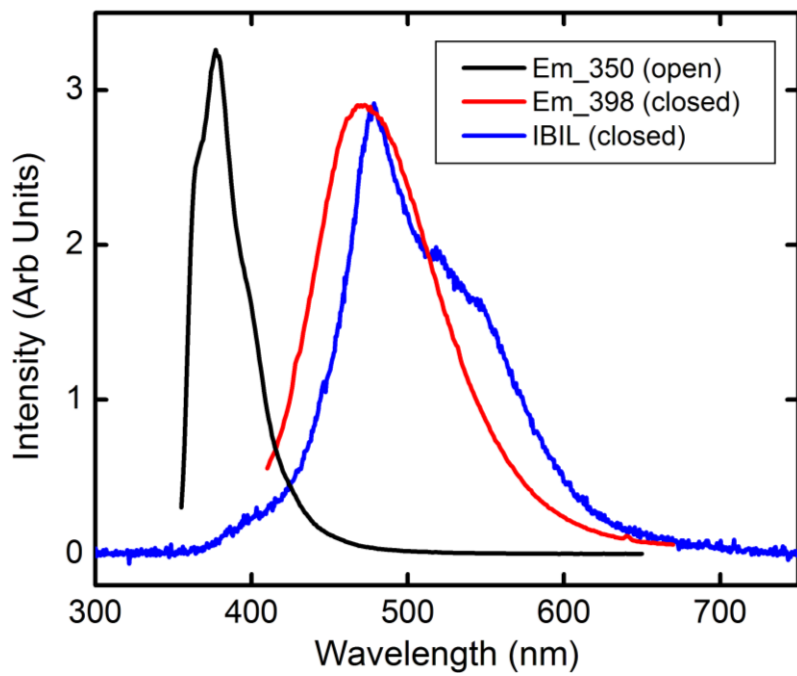
Figure 8. Comparison of the photoluminescence and proton-induced radioluminescence (IBIL) for 'open' and 'closed' frameworks DUT-4 (**1**) and MIL-69 (**2**), respectively.
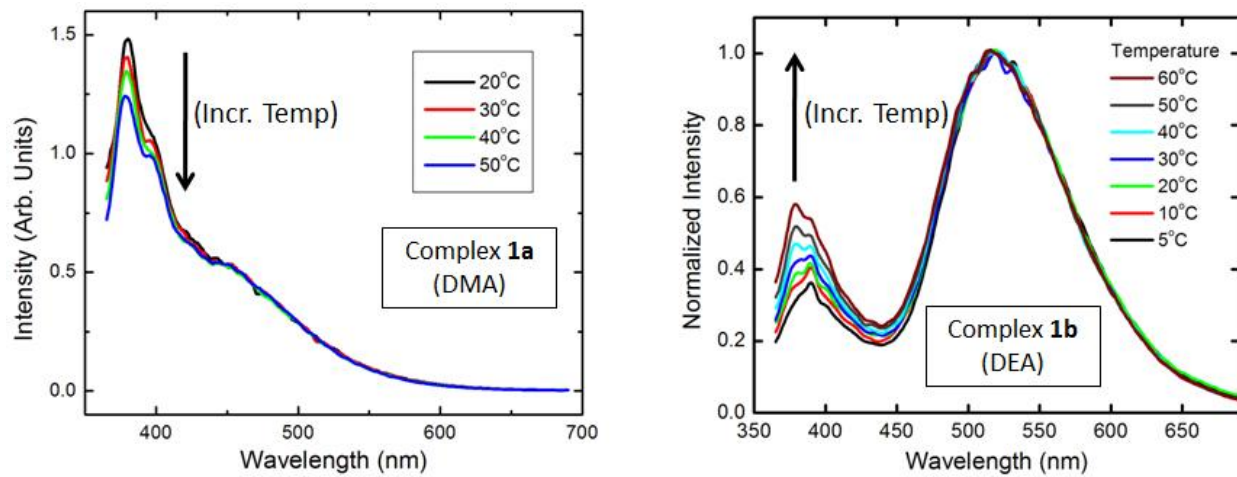
Figure 9. Temperature-dependent photoluminescence emission spectra for colloidal suspensions of compoounds **1a** and **1b** in cyclohexane.
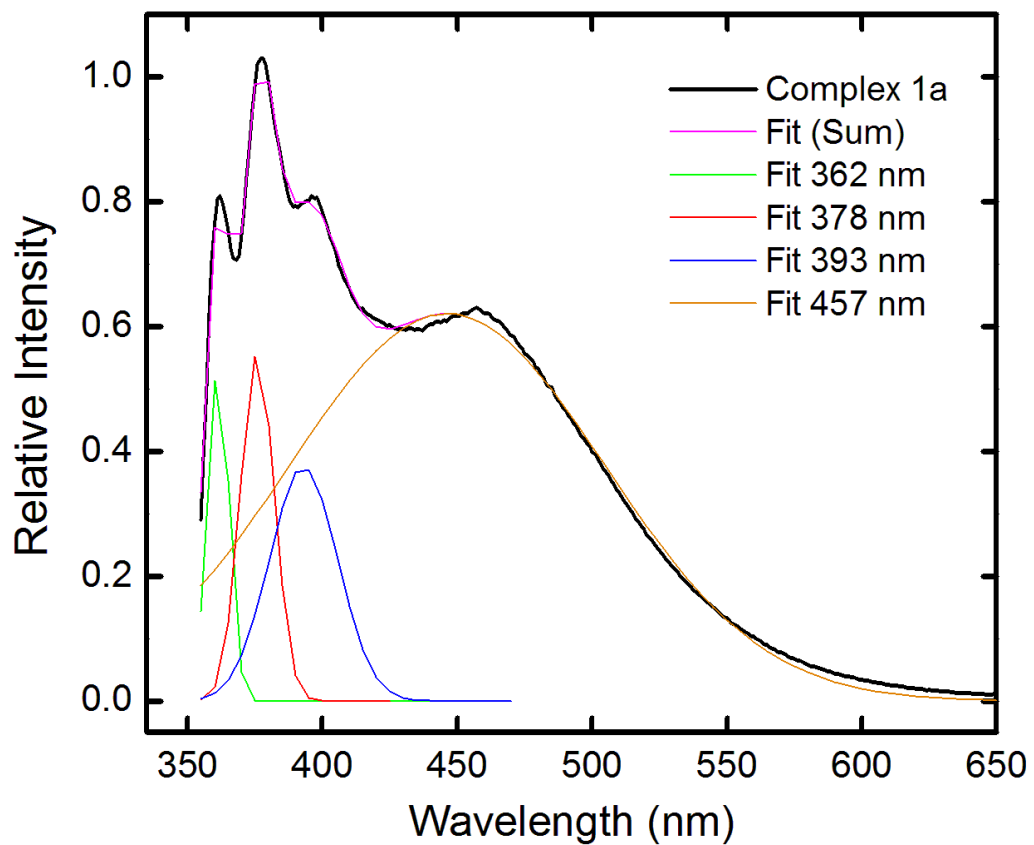
Figure 10. Gaussian fit to the photoluminescence spectrum of 1a, collected at λ_{ex}=340nm.
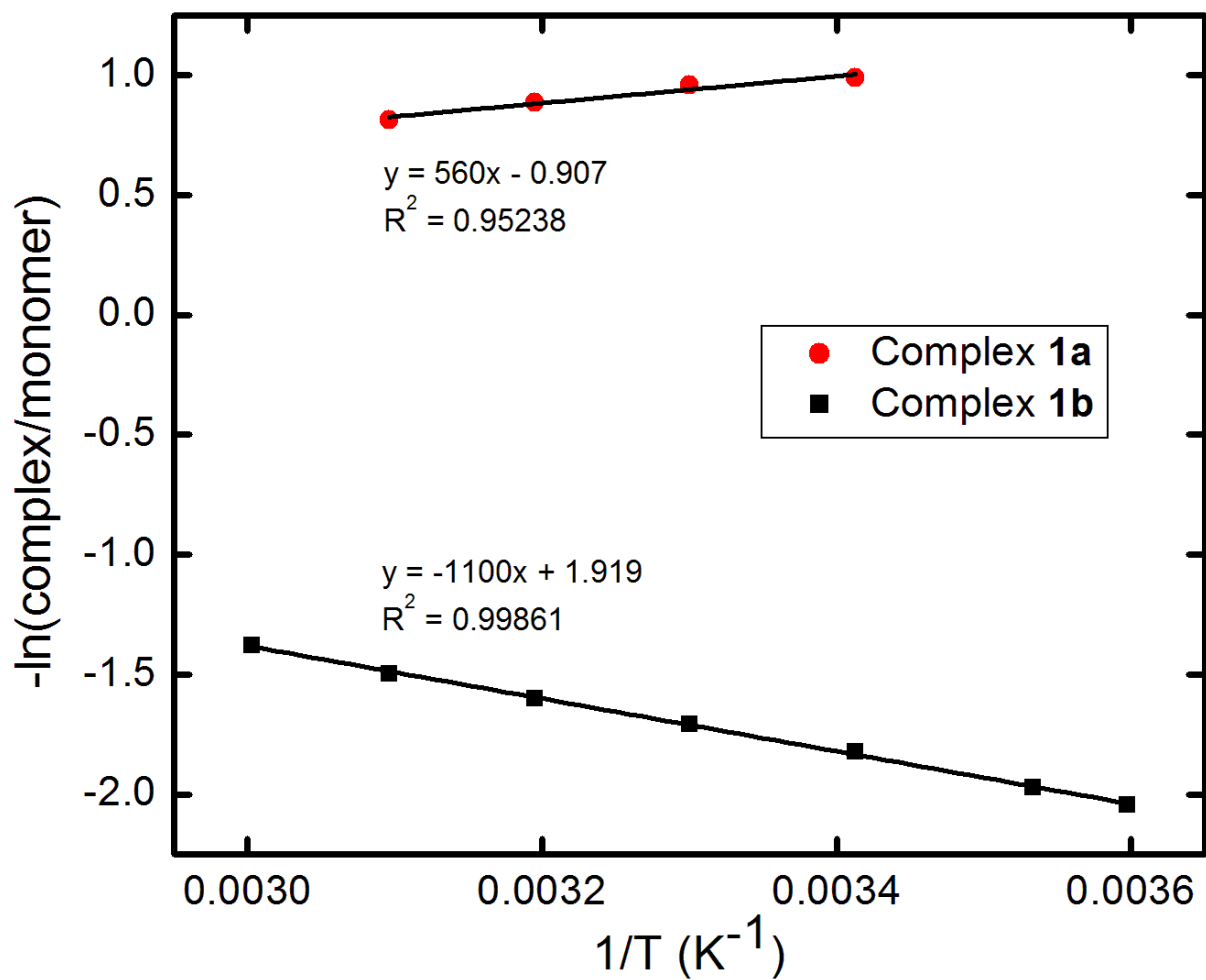
Figure 11. Intensity data from figure 10 plotted according to the equations: W1×(A1 + A2 + A3), monomer, and W2×(A4), exciplex, where W and A terms describe the peak weighting factors and amplitudes. The intensities were determined from the integrated Gaussian functions used to fit the monomer and CT emission bands (Figure S3).
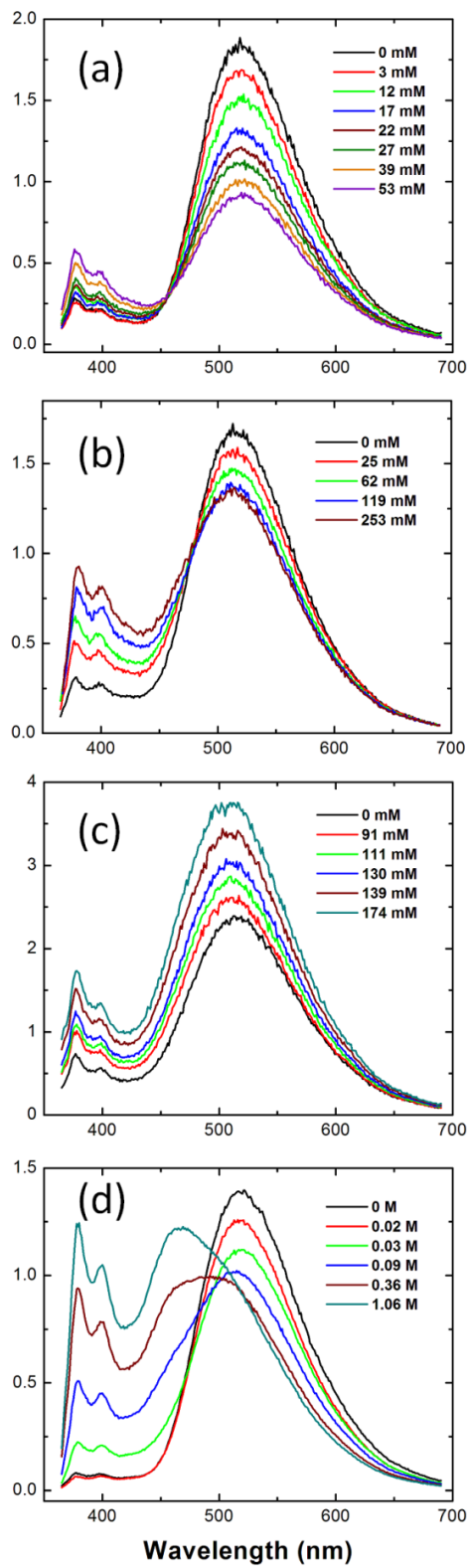
Figure 12. Solvent quenching-photoluminescence spectra of **1b** in (a) EtOH, (b) IPA, (c) toluene, and (d) chloroform.
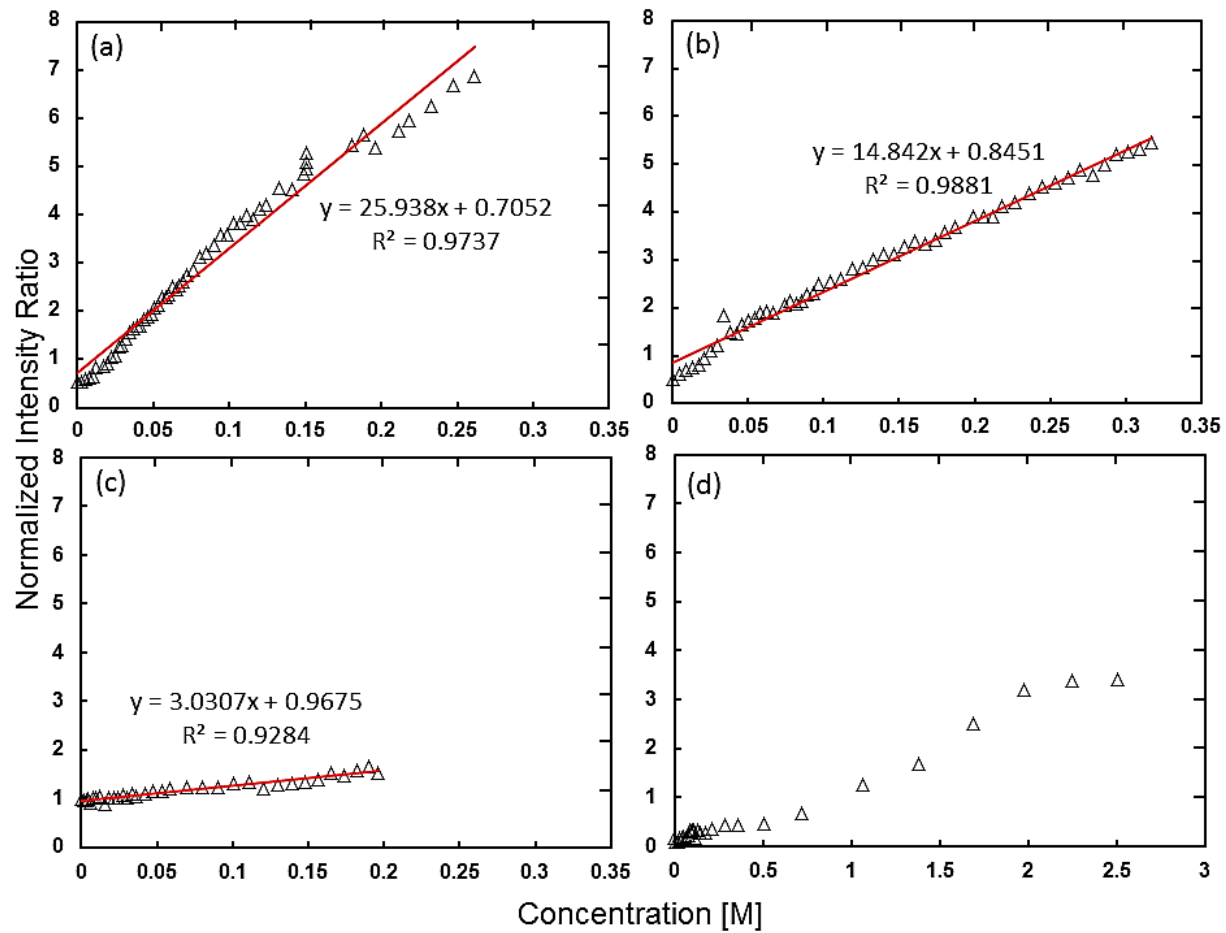
Figure 13. A plot of the intensity ratio of monomer: CT luminescence in **1b** as a function of the quencher concentration (a) EtOH, (b) IPA, (c) toluene, and (d) chloroform.
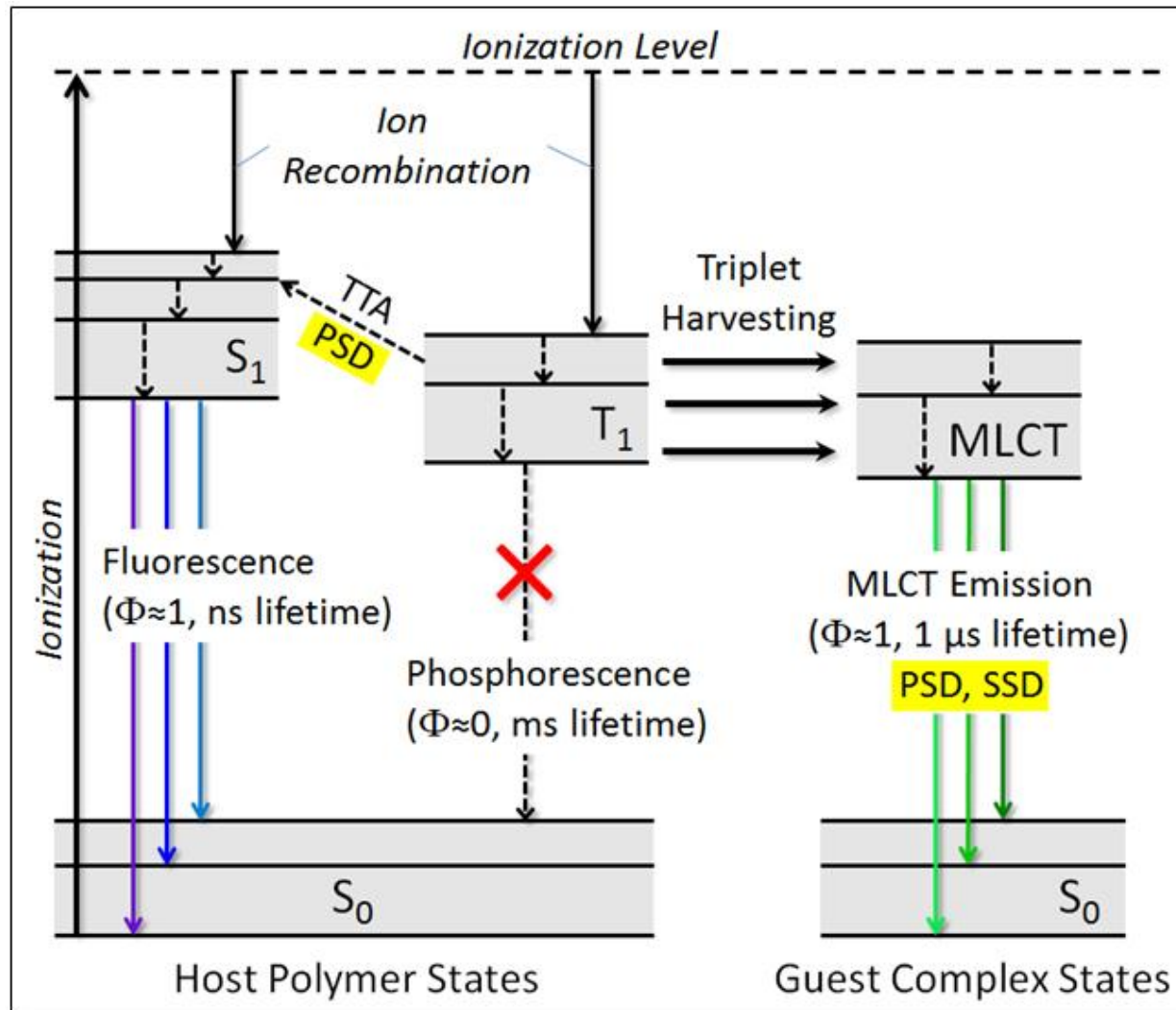
Figure 14. Jablonski energy level diagram describing the scintillation mechanism in traditional organic materials (left panel) and triplet-harvesting MOF scintillators (right panel). (TTA=triplet-triplet annihilation, PSD=pulse-shape discrimination, SSD=spectral-shape discrimination, MLCT=metal-to-ligand charge-transfer)
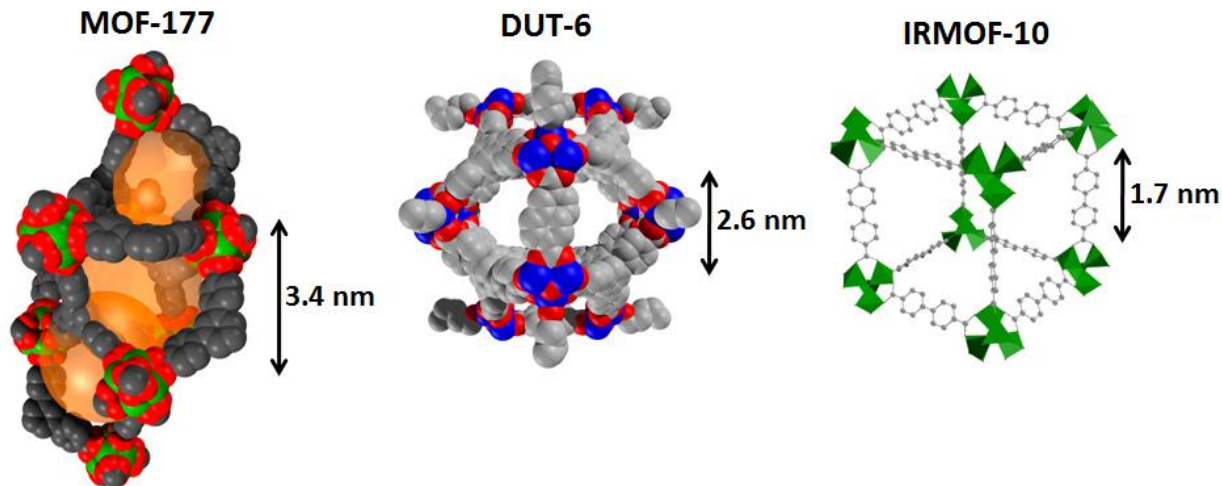
Figure 15. Comparison of the different cavity structures and sizes for three large-pore MOFs used in this study.
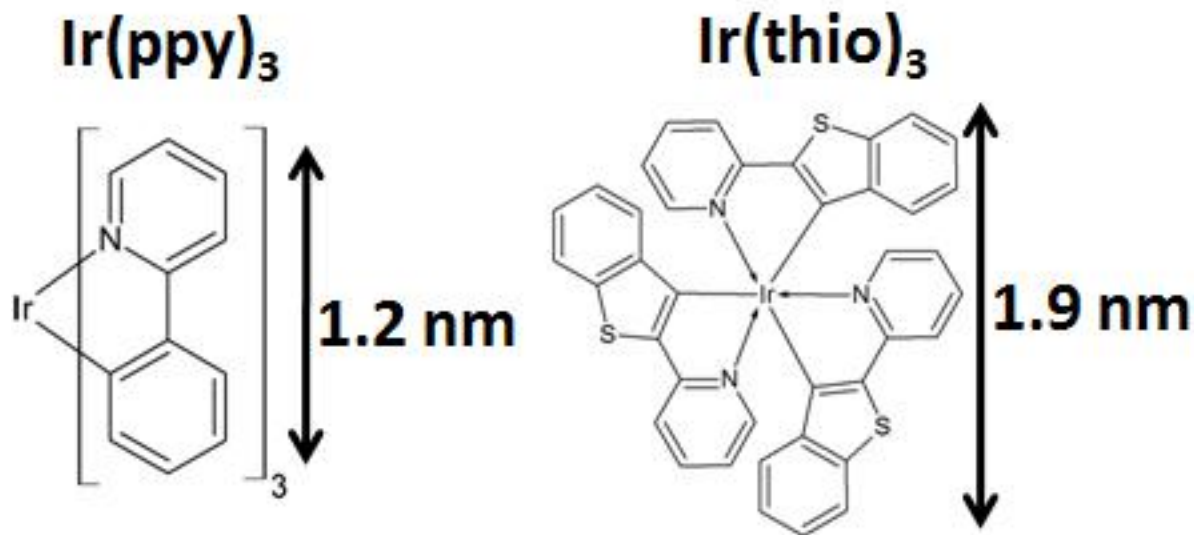
Figure 16. Molecular structures and van der Waal diameters for two Ir^{3+} organometallic complexes used in this study.
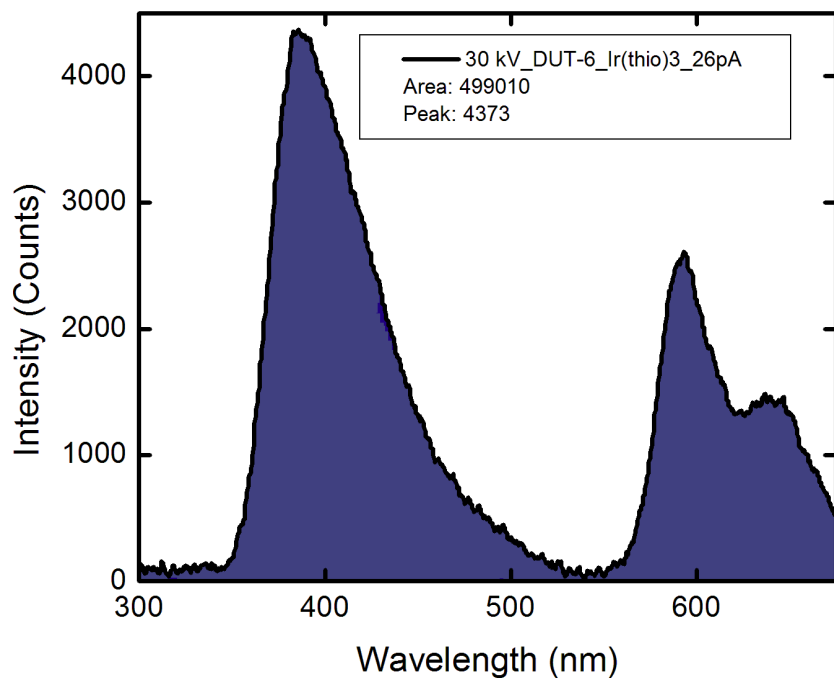
Figure 17. Proton radioluminescence emission spectrum of DUT-6 infiltrated with Ir(thio)₃, illustrating the unique spectral responses for singlet and triplet processes.
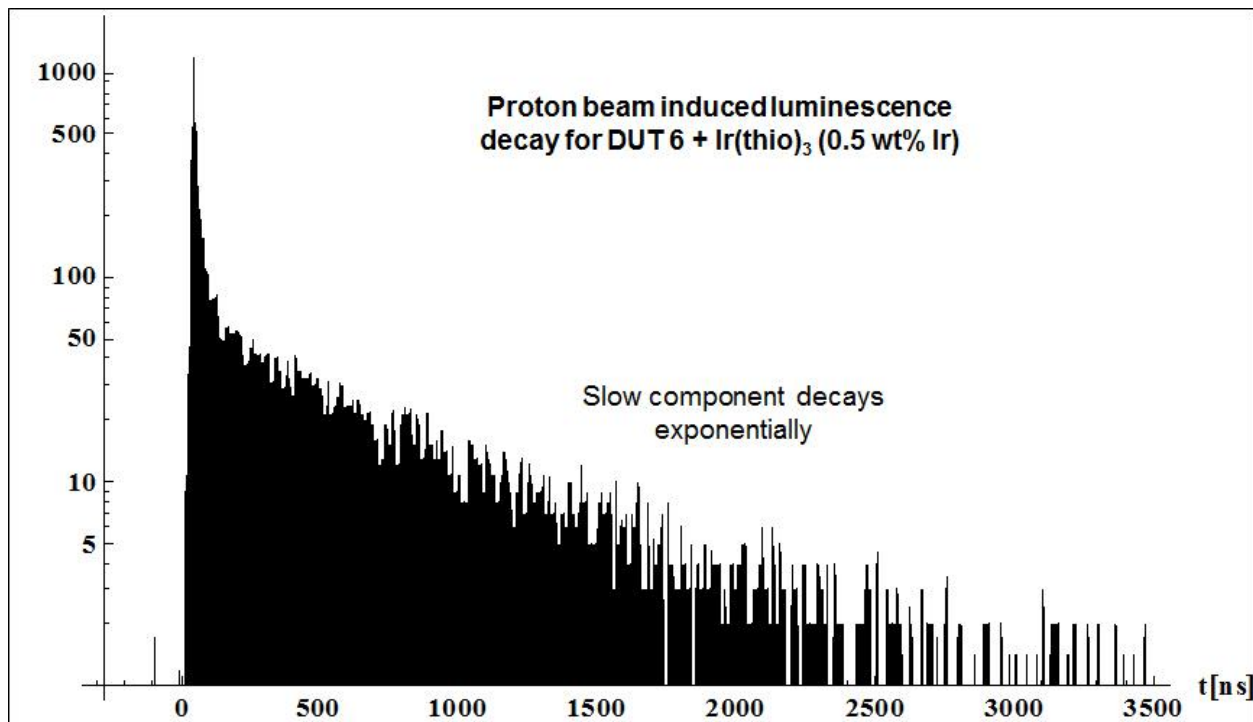

Figure 18. Proton radioluminescence decay curve obtained via time-correlated single-photon counting. Bi-exponential decay characteristics are observed corresponding to fast (host) MOF fluorescence and delayed (guest) phosphorescence.
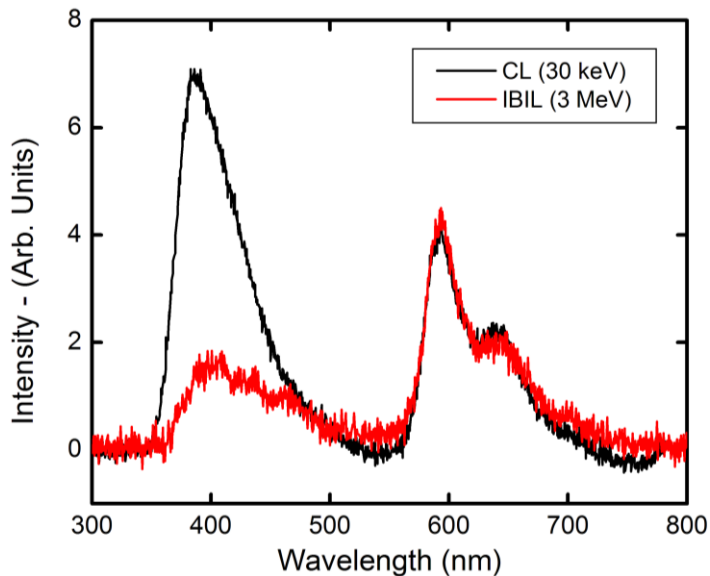
Figure 19. Cathodoluminescence (black) and proton radioluminescence (red) spectra for DUT-6 infiltrated with Ir(thio)$_3$, illustrating the concept of spectral-shape discrimination for electrons and protons.
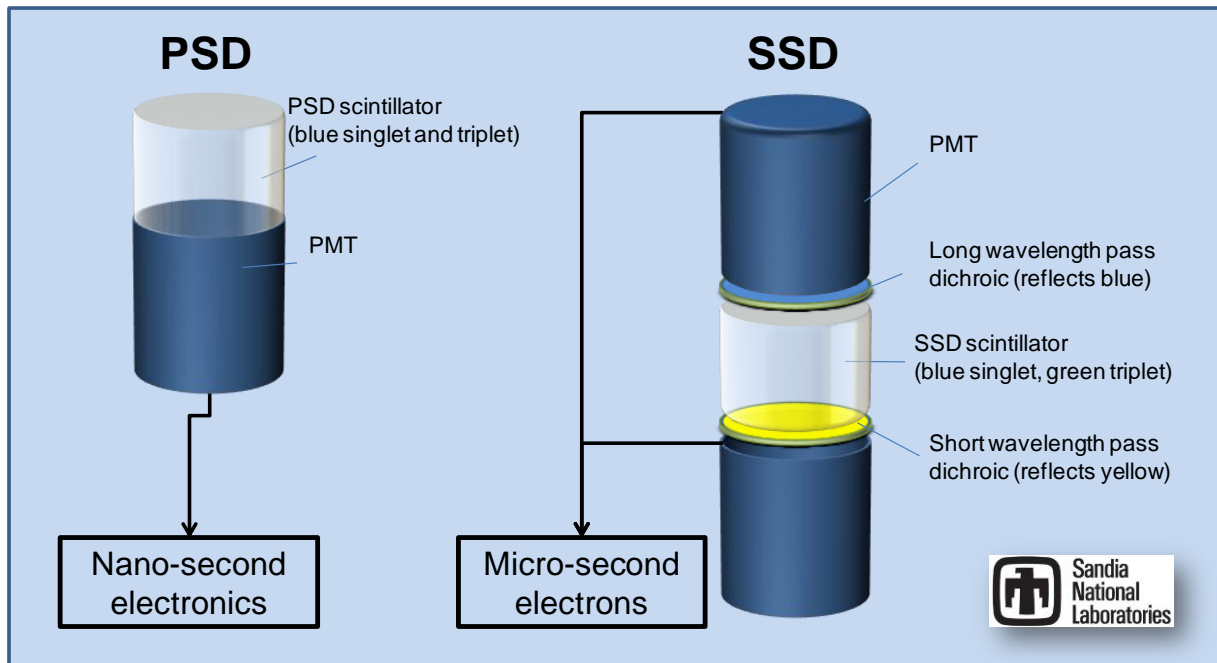

Figure 20. Spectral-shape discrimination (SSD) scheme contrasted with the detection set-up for pulse-shape discrimination (PSD) measurements.
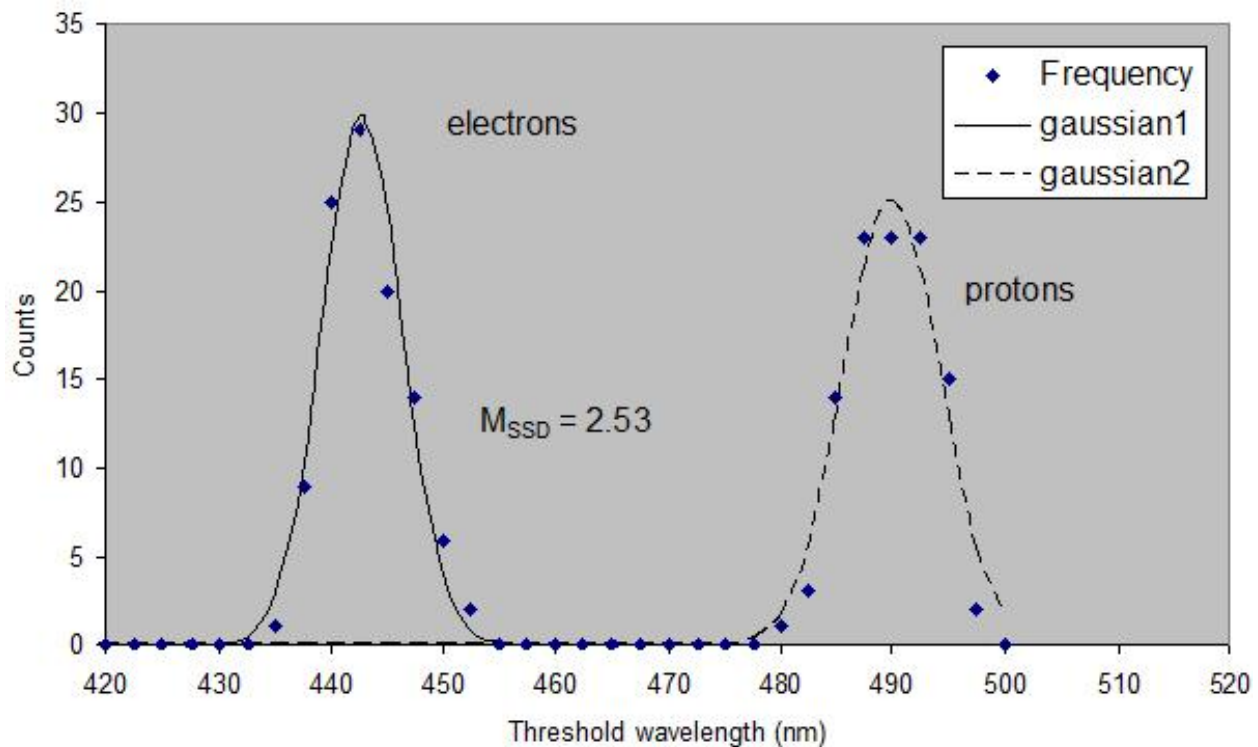
Figure 21. Spectral-shape discrimination histogram derived from steady-state radioluminescence data of DUT-6 infiltrated with Ir(ppy)$_3$.
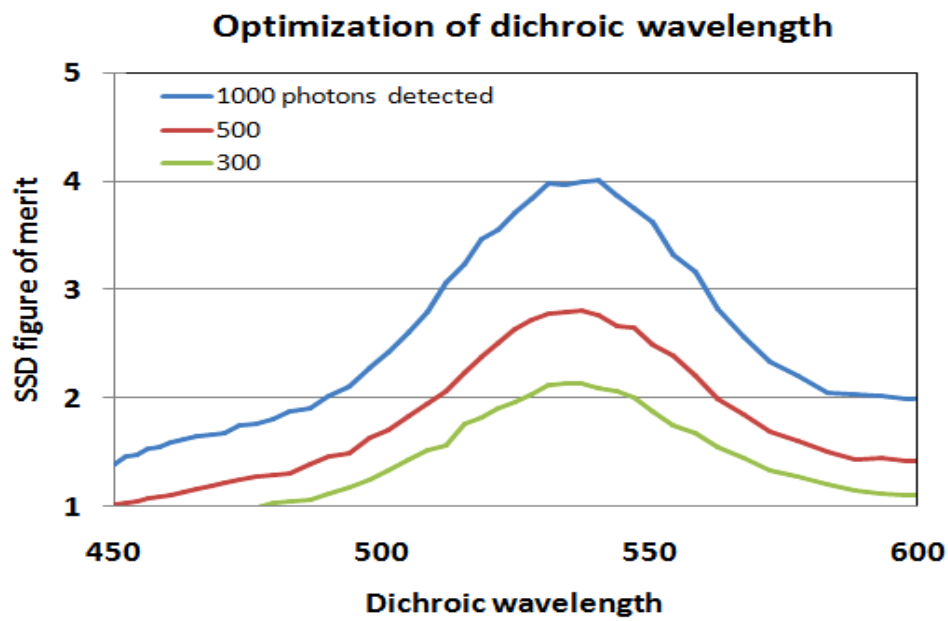

Figure 22. SSD-FOM plotted as a function of dichroic filter wavelength for different numbers of photons detected. These results were obtained for the steady-state spectra shown in Figure 19.
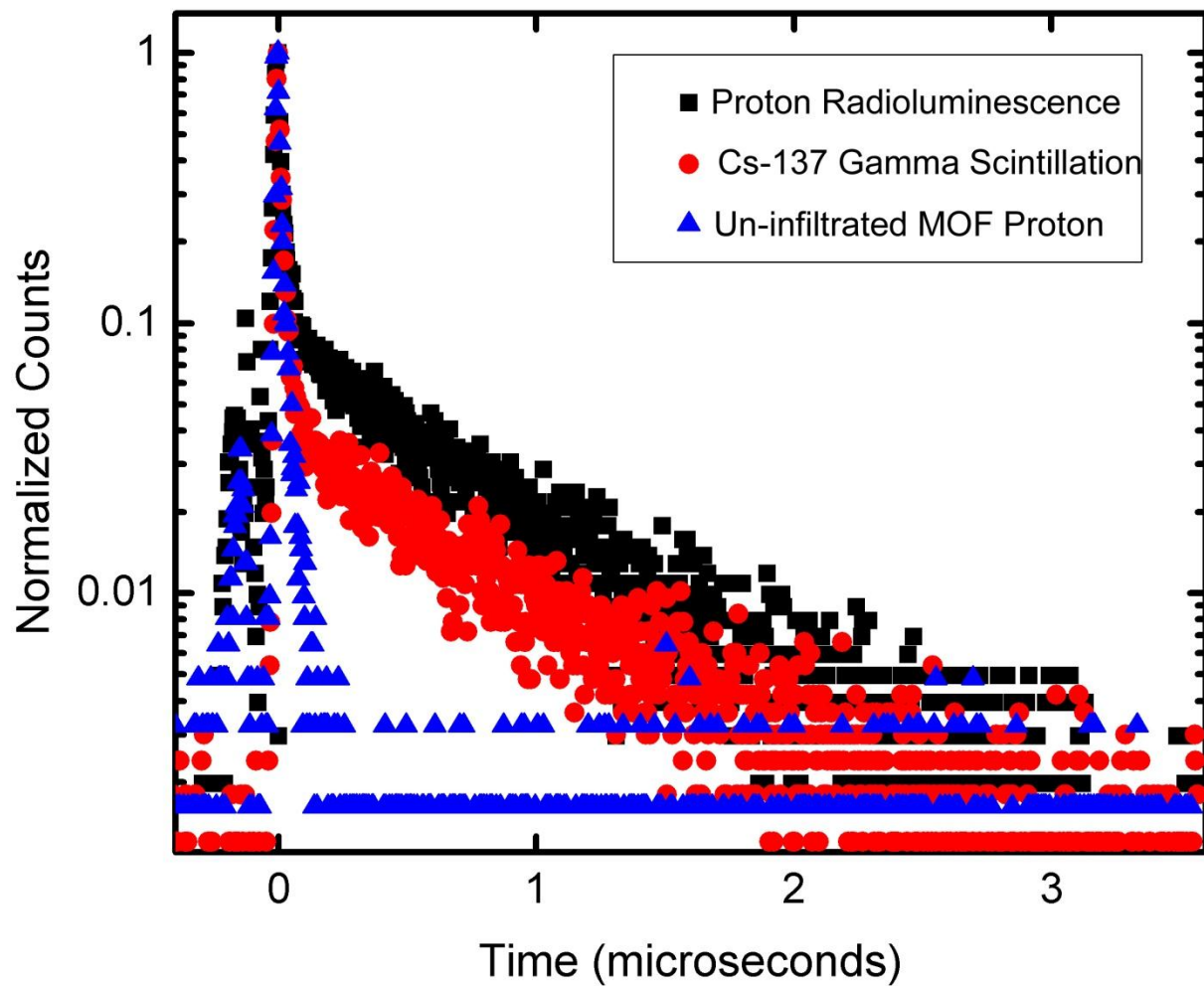
Figure 23. Cathodoluminescence (red) and proton radioluminescence (black) decay curves obtained using TCSPC. Differences in the relative proportion of prompt:delayed luminosity are evident in the average pulse shapes for different particle types.

DEPARTMENT OF DEFENSE

DEFENSE THREAT REDUCTION
AGENCY
8725 JOHN J. KINGMAN ROAD
STOP 6201
FORT BELVOIR, VA 22060
     ATTN: D. PETERSEN

DEFENSE TECHNICAL
INFORMATION CENTER
8725 JOHN J. KINGMAN ROAD,
SUITE 0944
FT. BELVOIR, VA 22060-6201
     ATTN: DTIC/OCA

DEPARTMENT OF DEFENSE
CONTRACTORS

QUANTERION SOLUTIONS, INC.
1680 TEXAS STREET, SE
KIRTLAND AFB, NM 87117-5669
     ATTN: DTRIAC